Supporting Information

Preparation of Nanoporous Graphene Oxide by Nanocrystal-masked Etching: Toward Nacre-mimetic Metal Organic Framework Molecular Sieving Membrane

*Yaoxin Hu,a Yueqin Wu,[b] Citsabehsan Devendran,[c] Jing Wei,[a] Yan Liang,[a] Masahiko Matsukata,[d] Wei Shen,[a] Adrian Neild,[c] Han Huang,[b] Huanting Wang,[a]**

[a] Department of Chemical Engineering, Monash University, Clayton, Victoria 3800, Australia, [b] School of Mechanical and Mining Engineering, The University of Queensland, St Lucia, QLD 4072, Australia, [c] Department of Mechanical and Aerospace Engineering, Monash University, Clayton, Victoria 3800, Australia, [d] Department of Applied Chemistry, Waseda University, Shinjuku Ku, Tokyo 1698555, Japan.

Address correspondence to huanting.wang@monash.edu

EXPERIMENTAL SECTION

Chemicals. Zn $(NO_3)_2 \cdot 6H_2O$ (98.0 wt. %, Sigma-Aldrich), 2-methylimidazole (Hmim, 99.0 wt. %, Sigma-Aldrich), methanol (analysis, Merck). All chemicals were used as provided. Porous anodic aluminium oxide (AAO) disks with a diameter of 13 mm (average pore diameter of 100 nm) from GE healthcare companies were used as supports.

Preparation of ZIF-8/MGO seeding layer. ZIF-8/GO nanosheets were prepared as previously reported earlier by our group.[1] Solutions of Zn $(NO_3)_2 \cdot 6H_2O$ (0.366 g) in 12 mL methanol, 2-methylimidazole (Hmim 0.811 g) in 20 mL methanol and 8 mL of GO suspension in mixture of methanol-water (4:1, v/v) were mixed together stirred for 3 h, leading to the formation of ZIF-8/GO nanosheets. The molar ratio of Hmim/Zn^{2+} in this system was 8. ZIF-8 nanoparticles were synthesized via the same process without the GO nanosheets. ZIF-8/GO seeding layer (denoted as S-3h-p0s) fabricated on an AAO disk via spin-coating of a stable ZIF-8/GO colloid suspension (0.02 g/ml) in methanol. Different irradiation times (10, 30, 60, 120 and 180 s) of oxygen plasma treatment of the ZIF-8/GO seeding layer were investigated, thus, the resultant ZIF-8/porous GO seeding layers (denoted as S-3h-p10s, S-3h-p30s, S-3h-p60s, S-3h-p120s and S-3h-p180s) were obtained respectively. Plasma treatment was carried out using Harrick Plasma PDC-32G-2 with 18 watts of power (max) at 1 mbar pressure. For the sake of comparison, pure porous GO film was prepared by spin-coating GO suspension on the AAO support followed by a 10 s oxygen plasma treatment. To compare with our nanocrystal-mask plasma etching method, the chemical etching method reported by Xu et al.[2] was used to produce porous GO nanosheets and then ZIF-8/porous GO nanosheets were synthesized by the same procedure using the obtained porous GO.

Fabrication of ZIF-8/MGO membrane. Ultrathin nacre-mimetic ZIF-8 membrane was prepared by secondarily growing the seeding layer coated on porous substrates *via* contra-diffusion method. [1] Zn^{2+} and Hmim solution were prepared by dissolving Zn $(NO_3)_2{\cdot}6H_2O$ (0.183g) and Hmim (0.405g) in 10 ml methanol, respectively. The coated support was mounted on a custom-made setup[3] vertically aligned, with the seeding layer facing the Zn^{2+} side, where the Zn^{2+} and Hmim solutions were separated by the coated support. After reaction at room temperature for 3 h, the ZIF-8 membranes from seeding layers were taken out and rinsed with fresh methanol. Lastly, the membranes were dried at 50 ºC overnight. In comparison, the ZIF-8 membrane was fabricated following the same synthesis process after 12 h reaction (contra-diffusion of Zn^{2+} and Hmim solutions) using the AAO support without seeding.

Characterization. Scanning electron microscopy (SEM) images were taken with a field-emission scanning electron microscopes (FEI Nova NanoSEM 450 and FEI Magellan 400) operating at 5 kV. Powder X-ray diffraction (PXRD) patterns were carried out in the 2θ range of 5-40° at room temperature using a Miniflex 600 diffractometer (Rigaku, Japan) in transmission geometry using Cu Kα radiation (15 mA and 40 kV) at a scan rate of 2 °/min with a step size of 0.02 °. X-ray photoelectron spectroscopy (XPS) experiments were recorded on a Kratos AXIS Ultra DLD system with Al Kα radiation as an X-ray source for radiation. The contact angle of the membranes was determined using a contact angle goniometer (Dataphysics OCA15, Dataphysics, Germany). FTIR spectra were recorded on a FT-IR spectrophotometer (PerkinElmer Spectrum 100, USA).

Gas permeation tests. All the gas permeance tests were performed in a custom-built apparatus via a constant–volume/variable-pressure method described in detail elsewhere. [3] The supported ZIF-8/MGO membranes were sealed on a stainless steel porous sample holder with a Varian Torr Seal vacuum sealant and placed in a larger Pyrex tube facing the feed gas flow. Moreover, the permeance side of the membrane connected to a MKS 628B Baratron pressure transducer and a vacuum pump. The gas permeance experiments were performed using steady-state gases (i.e. H_2, CO_2, N_2, CH_4, C_3H_6 and C_3H_8). For each single gas measurement, the permeate side of the membrane was thoroughly evacuated for approximately 30 mins, allowing enough time to reach steady-state permeation conditions. The molar flow rate (Ni) of the permeating gas was calculated from the linear pressure rise, and its coefficient was calibrated using a digital flowmeter (ADM2000, Agilent, California, USA). The feed gas is supplied at room temperature (25 ºC) under atmospheric pressure (1 bar). The permeate side in a vacuum condition, providing a driving force for permeation. The effective membrane area was measured. Membrane permeance, Pi (mol·m^{-2}·s^{-1}·pa^{-1}), is defined as (1).

$$\mathrm{P}_i = {}^{\mathrm{N}_i}\!\big/_{\Delta \mathrm{P}_i \cdot \mathrm{A}} \tag{1}$$

where Ni (mol·s^{-1}) is the molar flow rate of component i, ΔPi (Pa) is the transmembrane pressure difference of component i, and A (m^2) is the effective membrane area for testing. The ideal selectivity Si/j is calculated from the relation between the permeance of component i and component j.

$$S_{i/j} = {}^{\mathrm{P}_i}\!\big/_{\mathrm{P}_j} \tag{2}$$

Mechanical properties. The mechanical properties of membrane samples were characterized using nanoindentation. Nanoindentation tests were carried out on a Triboindenter (Hysitron Inc., Minneapolis, MN) equipped with a three-sided Berkovich indenter with a nominal tip radius of 100 nm and a total included angle of 142.3°. The samples were cut and attached to a steel stage using superglue. During indentation, for all tests, the loading, holding and unloading times were kept at 10, 10 and 15 seconds, respectively. The indentation peak load was varied from 200 μN to 4 mN. Load-displacement (*P-h*) curves were recorded. Prior to testing, the indenter was well calibrated using a standard quartz substrate. Morphologies of indentation impressions were characterized using *in situ* Atomic Force Microscopy (AFM). Hardness values of the membrane samples were calculated from the *P-h* curves using the Oliver-Pharr method.[4] To eliminate the substrate effect, a series of indentations with loads varied from 200 μN to 4 mN were employed using an empirical deconvolution method[5] to obtain the mechanical properties of the top selective layer.

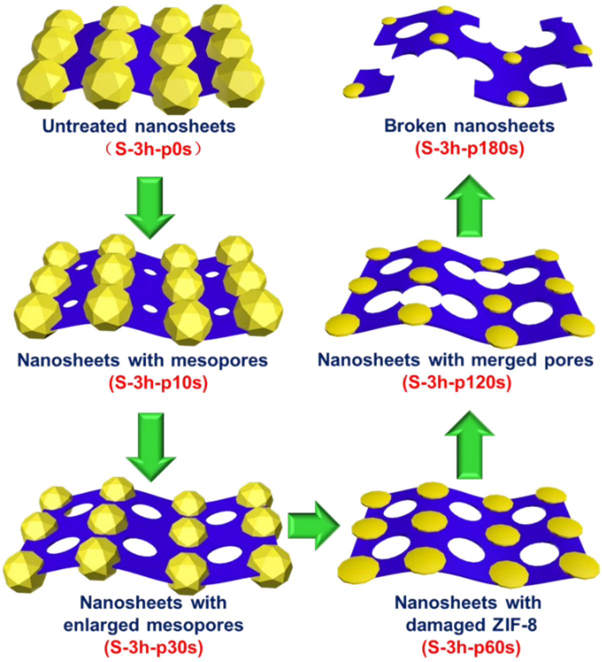

Figure S1 Schematic illustration of nanocrystal-mask plasma etching process under different duration of plasma irradiation.

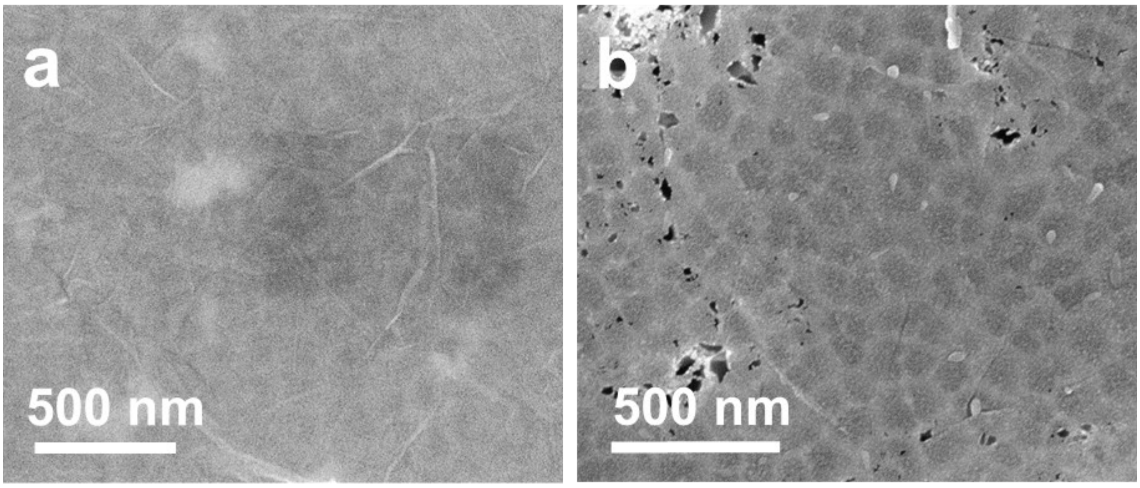

Figure S2 SEM images of surface of oxygen plasma treated pure GO film.

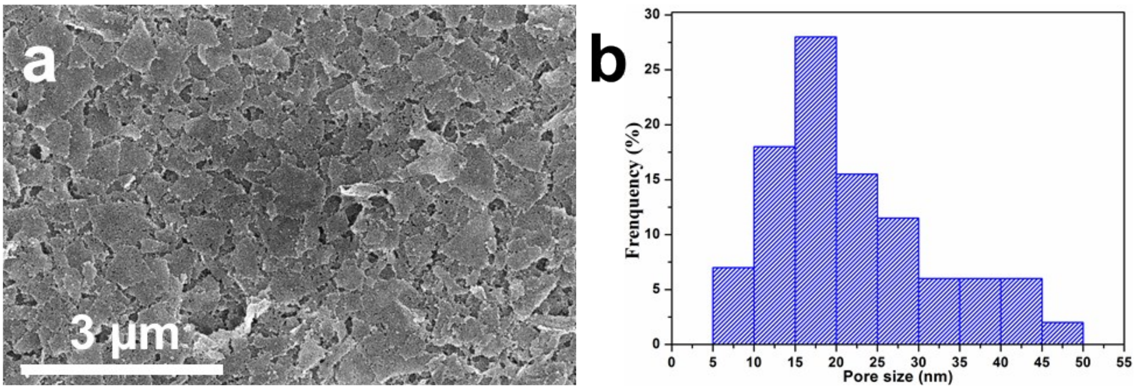

Figure S3 a) SEM image and b) pore size distribution of ZIF-8/MGO nanosheets (S-3h-p30s).

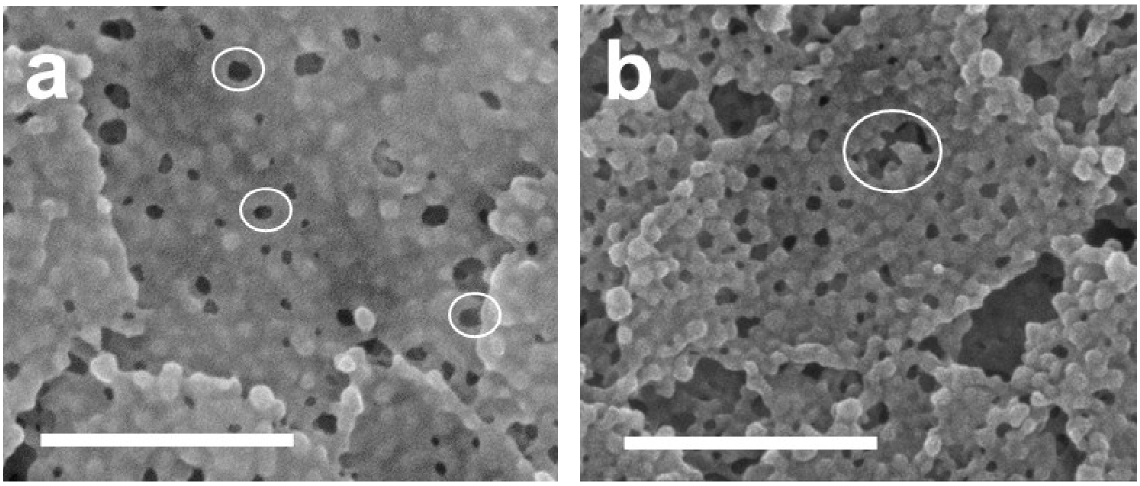

Figure S4 SEM images of ZIF-8/GO scaffold seeding layers (S-3h-P60s and S-3h-P120s) post-exposure of oxygen plasma corresponding to a) 60 and b) 120 s. A few pores are white-circled on the SEM images to guide the eye. All scale bars are 300 nm.

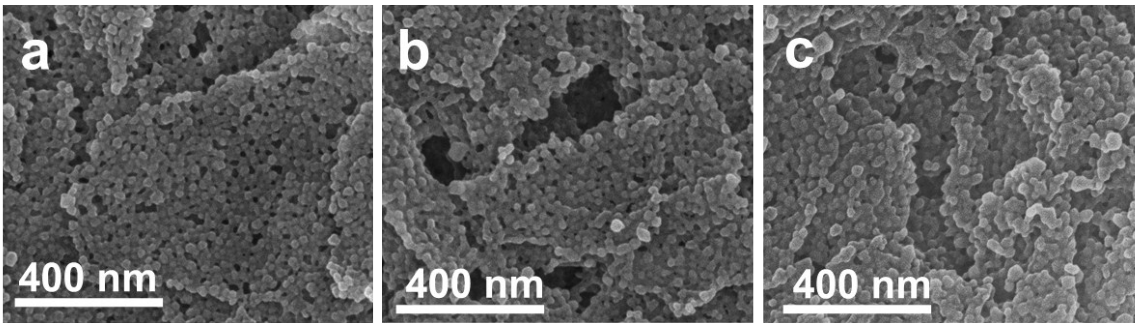

Figure S5 SEM images of ZIF-8/MGO seeding layer with the different coverage of ZIF-8 crystals, a) S-3h-p30s, b) S-5h-p30s and c) S-26h-p30s.

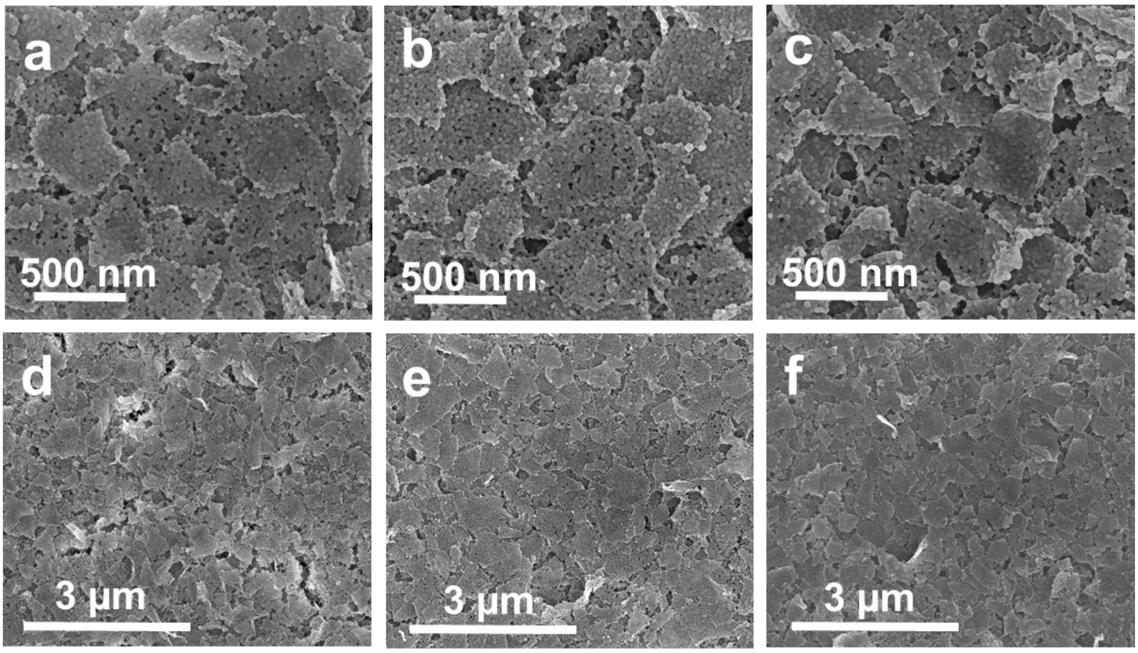

Figure S6 SEM images of ZIF-8/MGO seeding layers with different ZIF-8 crystal coverage after prolonged exposure of 60 s plasma treatment, a,d) S-3h-p60s, b,e) S-5h-p60s, and c,f) S-26h-p60s.

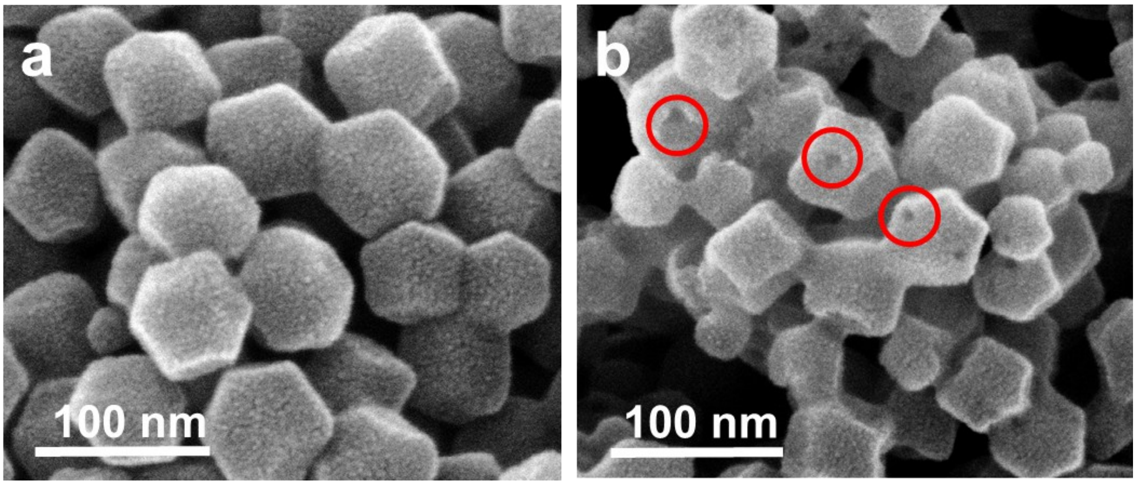

Figure S7 SEM images of a) untreated and b) post-treated of ZIF-8 nanoparticles. The red circles in the images highlight a few typical defects.

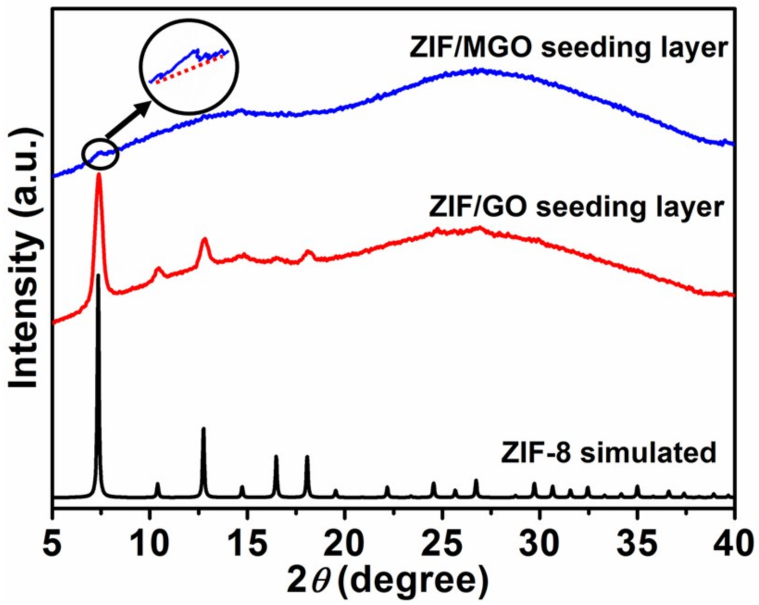

Figure S8 XRD patterns of simulated ZIF-8 structure, untreated and post-treated by 30 s plasma etching of thick ZIF-8/MGO seeding layer (S-3h-C5-p30s). The inset depicts a magnification of the XRD pattern

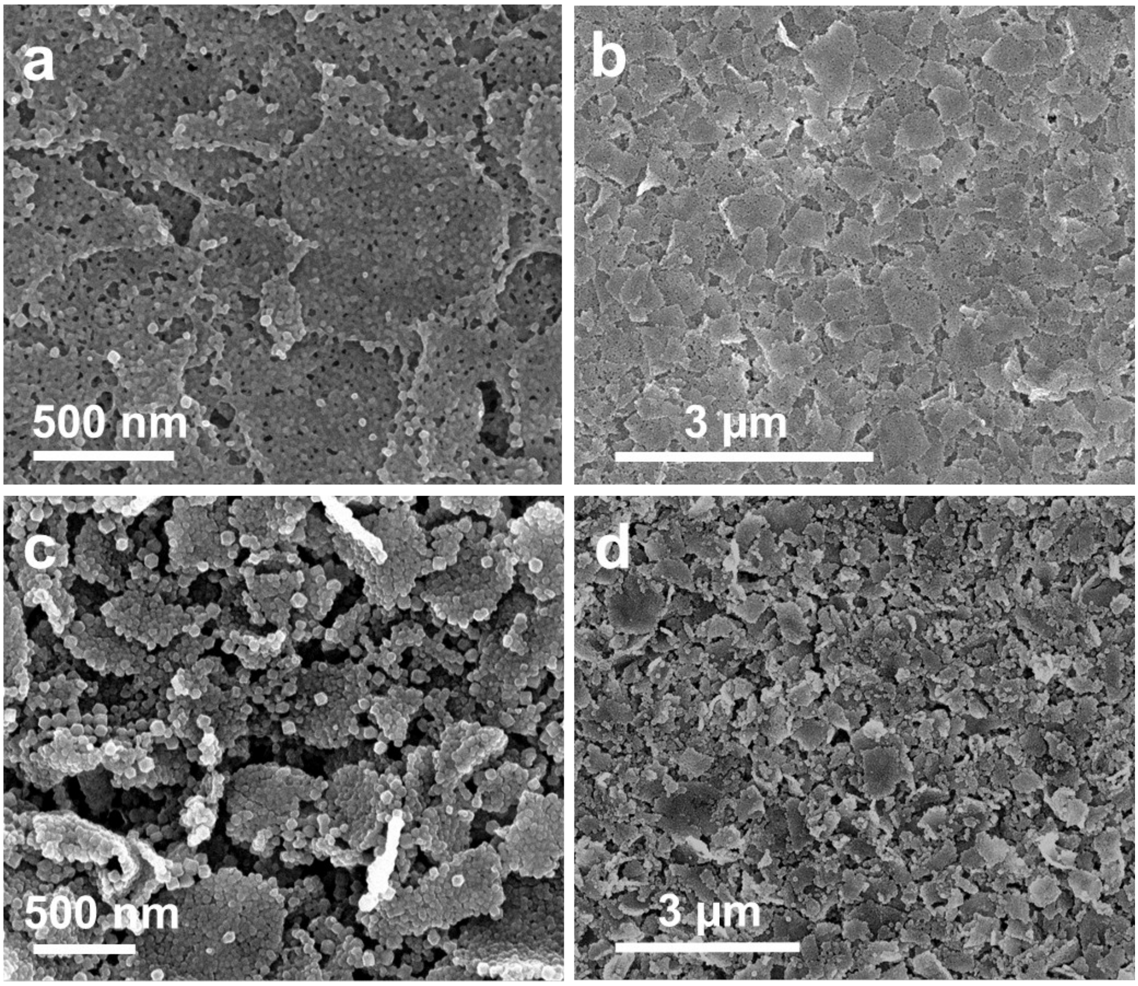

Figure S9 SEM images of ZIF-8/porous GO nanocomposites fabricated through a-b) nanocrystal-mask plasma etching (S-3h-p30s) and c-d) chemical etching method.

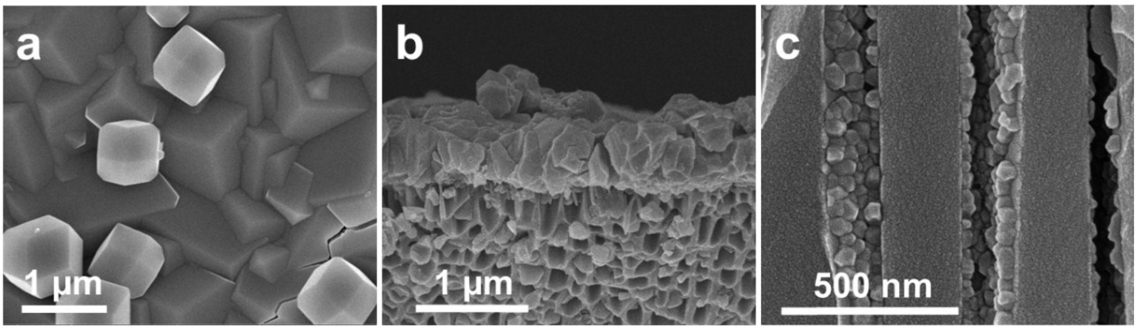

Figure S10 SEM images of the a) surface and b-c) cross-section of ZIF-8 membrane via contra-diffusion method. ZIF-8 nanoparticles formed in the channel of the substrate and grain boundary defects are shown in ZIF-8 membrane.

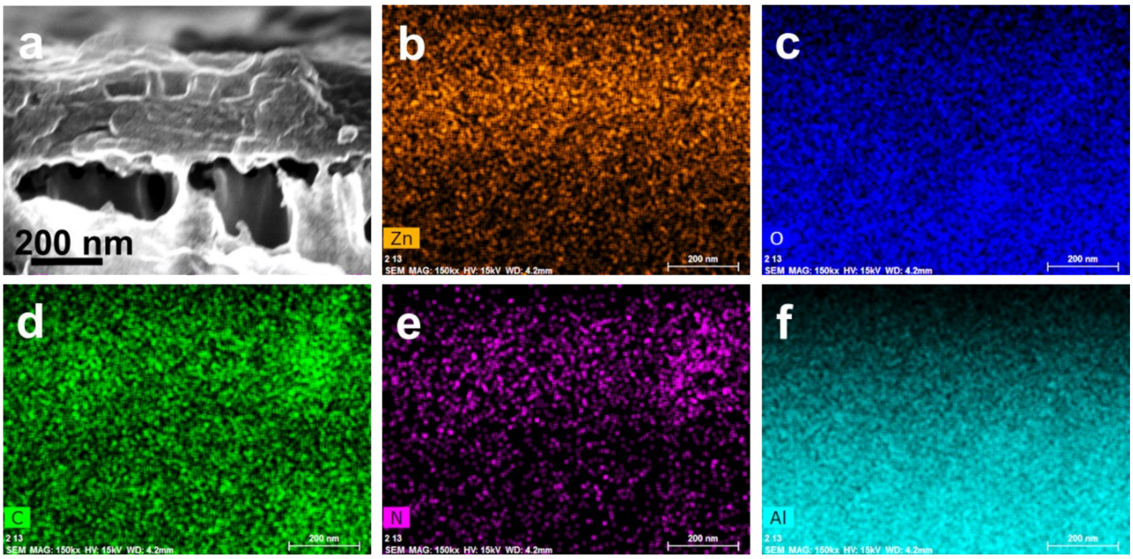

Figure S11 SEM image (a) and EDX elemental mapping of the cross section of a ZIF-8/MGO membrane (M-3h-p30): Zn (b), O(c), C(d), N(e) and Al(f).

Because the thickness of between different ZIF layers is around few tens of nanometers, EDX elemental mapping images cannot show clearly edge of different ZIF layer. From EDX mapping images, oxygen element is uniformly distributed in the membrane structure, which indicates uniform dispersion of MGO nanosheets in the ZIF-8 polycrystalline film.

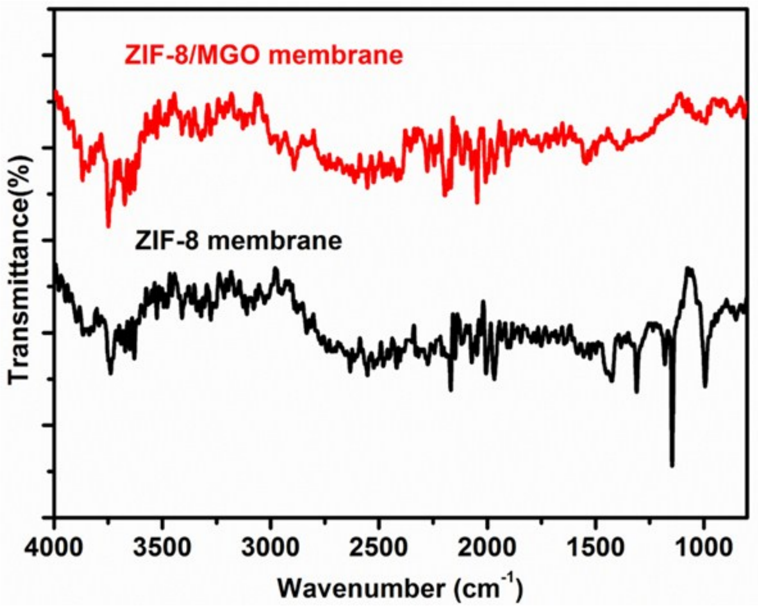

Figure S12 FTIR spectra of ZIF-8 and ZIF-8/MGO membrane (M-3h-p30).

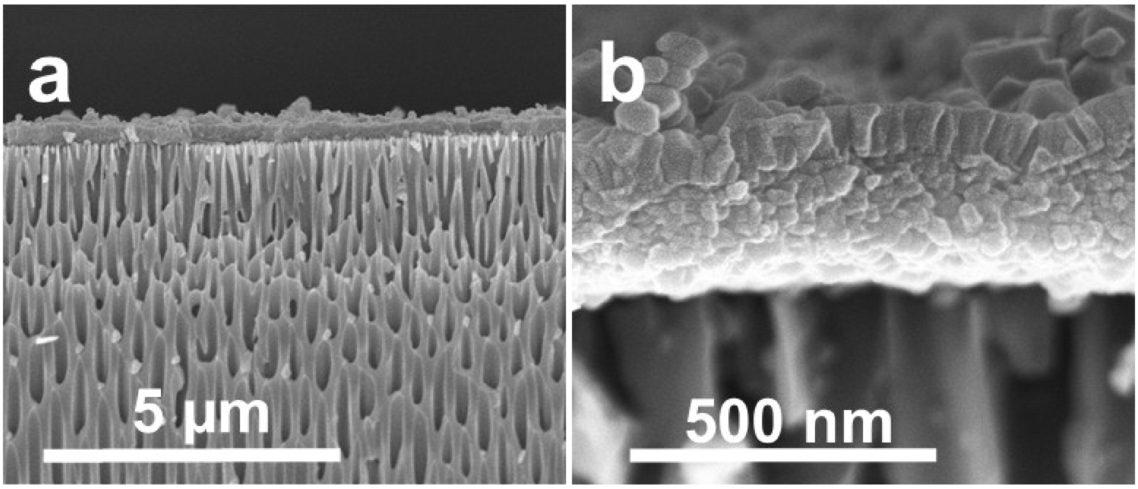

Figure S13 SEM images of the cross-section of ZIF-8/MGO membrane (S-3h-p30s), a) low magnification and b) high magnification.

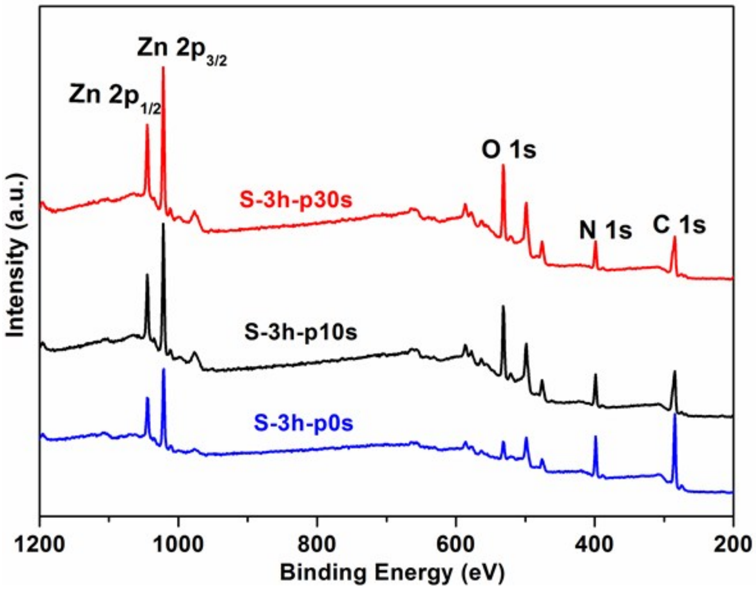

Figure S14 X-ray photoelectron spectroscopy (XPS) survey spectra spectra of ZIF-8/GO (S-3h-p0s), ZIF-8/MGO(S-3h-p10s) and ZIF-8/MGO(S-3h-p30s) seeding layer on AAO support.

Table 1 Atomic percentage of the element consisting of ZIF-8/GO (S-3h-p0s), ZIF-8/MGO(S-3h-p10s) and ZIF-8/MGO(S-3h-p30s) seeding layer on AAO support (atom% from XPS analysis).

Sample	Element (Atom %)			
	C	N	O	Zn
S-3h-p0s	70.53	20.15	6.31	3.01
S-3h-p10s	54.73	16.45	24.40	4.42
S-3h-p30s	53.43	15.23	26.14	5.19

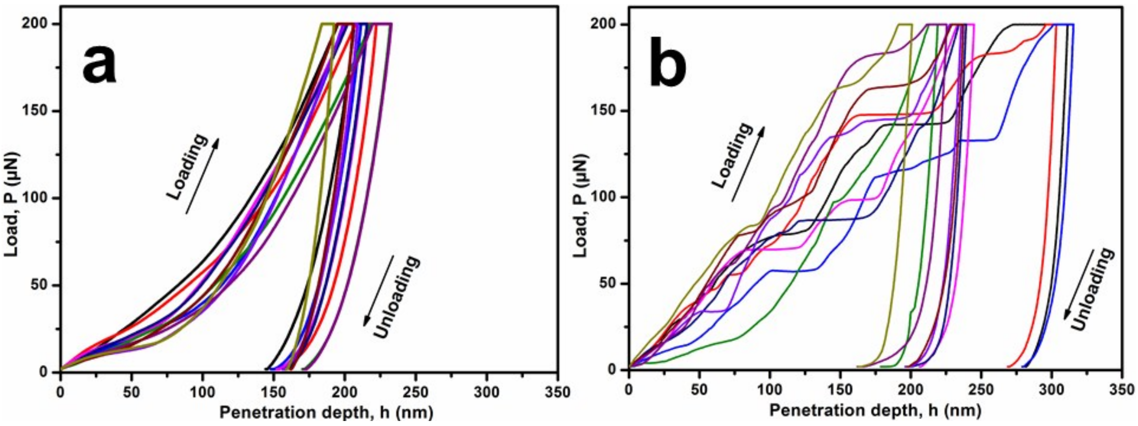

Figure S15 The load-displacement (*P*-*h*) curves at the same indentation load of 200μN for (a) the ZIF-8/MGO membrane (M-3h-p30) and (b) pure ZIF-8 membrane.

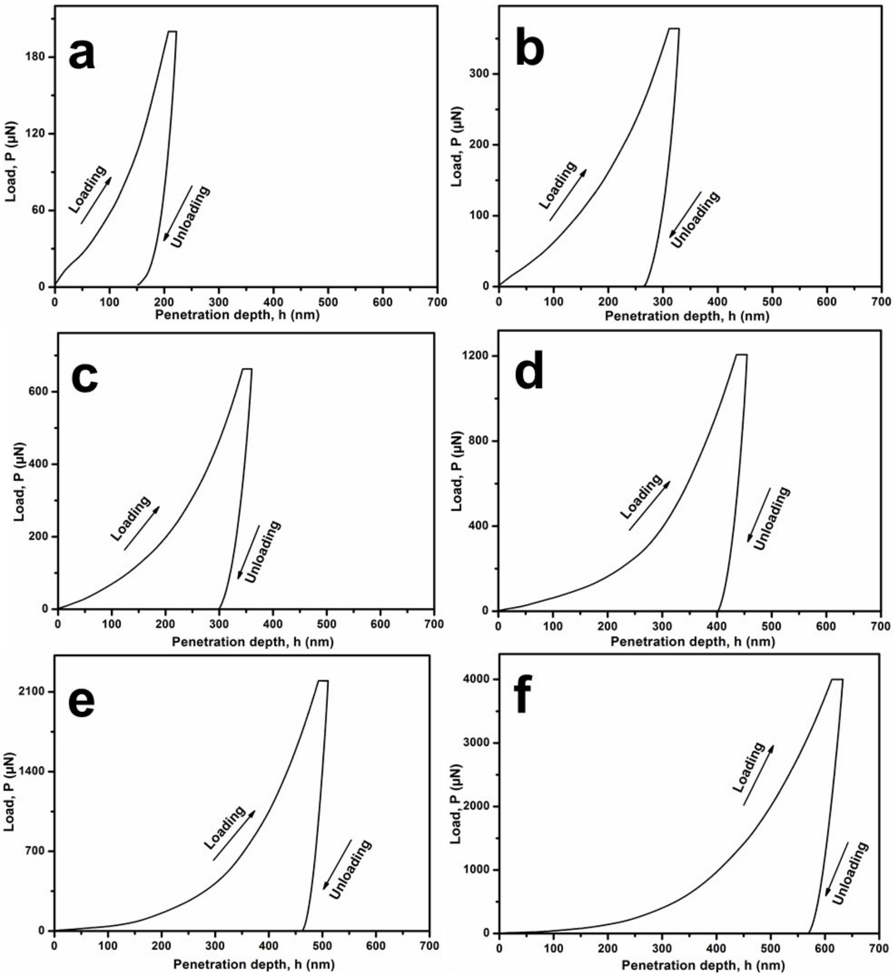

Figure S16 The load-displacement curves for ZIF-8/MGO membrane (M-3h-p30s) obtained at different indentation loads of (a) 200 μN, (b) 360 μN, (c) 660 μN, (d) 1200 μN, (e) 2200 μN and (f) 4000 μN.

Table S2. Single permeances and ideal selectivity of different ZIF/GO membrane and ZIF/MGO membrane measured at 25 °C and 1 bar

Membrane	Plasma irradiation time of seeding layer	Idea selectivity (H_2/N_2)	Permeance（10^{-8} mol $m^{-2}s^{-1}pa^{-1}$）	
			H_2	N_2
M-3h-p0s	0s	11.1	5.46	0.49
M-3h-p10s	10s	9.8	19.54	1.99
M-3h-3h	30s	10.0	117.55	11.7

Table S3. Single gas permeance and ideal selectivity for the ZIF-8/MGO membrane prepared on AAO disk (M-3h-p30s) at 25 °C and 1 bar

Gas $_{i/j}$	Knudsen constant	Permeance（10^{-8} mol $m^{-2}s^{-1}pa^{-1}$）		Ideal selectivity (S $_{i/j}$)
		Permeances (i)	Permeances (j)	
H_2/CO_2	4.7	117.55	35.84	3.3
H_2/N_2	3.7	117.55	11.77	10.0
H_2/CH_4	2.8	117.55	11.25	10.4
H_2/C_3H_6	4.6	117.55	1.73	67.9
H_2/C_3H_8	4.7	117.55	0.049	2409
C_3H_6/C_3H_8	1.02	1.73	0.049	35

Table S4. Comparison of the gas separation properties of the ZIF-8/MGO membrane (M-3h-p30s) with other membranes from the recent literature

Membrane	**Membrane thickness (μm)**	**Gas separation performance**				**Reference**
		Temperature (°C)	**Selectivity**		**H_2 Permeance (10^{-8} mol $m^{-2}s^{-1}Pa^{-1}$)**	
			H_2/C_3H_8	**C_3H_6/C_3H_8**		
ZIF-8	12	25	300[a]	-	8[a]	*Chem. Mater.* [6]
ZIF-8	2	25	501	14	35	*Chem.Commun* [7]
ZIF-8	20	150	905.1	13.6	21.7	*J. Am.Chem. Soc.* [8]
ZIF-8	15	150	37.8	-	34	*Microporous Mesoporous Mater.* [9]
ZIF-8	2	25	1100	-	154	*J. Membr. Sci.* [10]
ZIF-8	0.5-1	25	111	3.5	1.9	*Chem.Commun* [11]
ZIF-8	8.8	25	250[a]	12[a]	16[a]	*Science* [12]
ZIF-8	8	25	~1450[a]	65[a]	~42[a]	*Adv. Funct. Mater.* [13]
ZIF-8	2	25	833	16	75	*ACS Appl. Mater. Interfaces* [14]
ZIF-8@GO	20	250	5870	-	14.5	*J. Am.Chem. Soc.* [15]
ZIF-8/GO	0.1	25	405	12	5.5	*Angew. Chem. Int. Ed.* [1]
ZIF-95	30	325	66.8	-	246	*Chem.Commun* [16]
ZIF-90	20	225	456	-	28.5	*Microporous Mesoporous Mater.* [17]
IRMOF-3	10	25	2.4	-	110	*Langmuir* [18]
LTA $AlPO_4$	20	20	181	-	26	*J. Am.Chem. Soc.* [19]
Silica	10	250	150	-	1.53	*Microporous Mesoporous Mater* [20]
Ag-LTA	5	50	284	-	23	*J. Membr. Sci.* [21]
SAPO-34	4	25	26.5	-	696	*Int J Hydrogen Energy* [22]
ITQ-29	12	300	145.1	-	36	*Chem.Commun* [23]
ZIF-8/MGO	**0.43**	**25**	**2409**	**35**	**117.6**	**This work**

a) (mixture gas separation performance)

REFERENCES

1. Y. X. Hu, J. Wei, Y. Liang, H. C. Zhang, X. W. Zhang, W. Shen and H. T. Wang, *Angew. Chem.-Int. Edit.*, 2016, **55**, 2048-2052.
2. Y. Xu, C. Y. Chen, Z. Zhao, Z. Lin, C. Lee, X. Xu, C. Wang, Y. Huang, M. I. Shakir and X. Duan, *Nano Lett.*, 2015, **15**, 4605-4610.
3. J. Yao, D. Dong, D. Li, L. He, G. Xu and H. Wang, *Chem. Commun.*, 2011, **47**, 2559-2561.
4. W. C. Oliver, *J Mater Res*, 1992, **7**, 1564-1583.
5. Y. G. Jung, B. R. Lawn, M. Martyniuk, H. Huang and X. Z. Hu, *J Mater Res*, 2004, **19**, 3076-3080.
6. H. Bux, A. Feldhoff, J. Cravillon, M. Wiebcke, Y. S. Li and J. Caro, *Chem. Mater*, 2011, **23**, 2262-2269.
7. Y. Pan and Z. Lai, *Chem. Commun.*, 2011, **47**, 10275-10277.
8. Q. Liu, N. Wang, J. Caro and A. Huang, *J. Am. Chem. Soc.*, 2013, **135**, 17679-17682.
9. J. Yang, Z. Xie, H. Yin, J. Wang, J. Xu, J. Wang, J. Lu, D. Yin and Y. Zhang, *Microporous Mesoporous Mater.*, 2014, **198**, 263-270.
10. Y. Pan, B. Wang and Z. Lai, *J. Membr. Sci.*, 2012, **421-422**, 292-298.
11. O. Shekhah, R. Swaidan, Y. Belmabkhout, M. Du Plessis, T. Jacobs, L. J. Barbour, I. Pinnau and M. Eddaoudi, *Chem. Commun.*, 2014, **50**, 2089-2092.
12. A. J. Brown, N. A. Brunelli, K. Eum, F. Rashidi, J. R. Johnson, W. J. Koros, C. W. Jones and S. Nair, *Science*, 2014, **345**, 72-75.
13. K. Eum, A. Rownaghi, D. Choi, R. R. Bhave, C. W. Jones and S. Nair, *Adv. Funct. Mater.*, 2016, **26**, 5011-5018.
14. E. Shamsaei, X. Lin, Z. X. Low, Z. Abbasi, Y. Hu, J. Z. Liu and H. Wang, *ACS Appl. Mater. Interfaces*, 2016, **8**, 6236-6244.
15. A. Huang, Q. Liu, N. Wang, Y. Zhu and J. Caro, *J. Am. Chem. Soc.*, 2014, **136**, 14686-14689.
16. A. Huang, Y. Chen, N. Wang, Z. Hu, J. Jiang and J. Caro, *Chem. Commun.*, 2012, **48**, 10981-10983.
17. A. Huang, Q. Liu, N. Wang and J. Caro, *Microporous Mesoporous Mater.*, 2014, **192**, 18-22.
18. Y. Yoo, V. Varela-Guerrero and H. K. Jeong, *Langmuir*, 2011, **27**, 2652-2657.
19. A. Huang, F. Liang, F. Steinbach, T. M. Gesing and J. Caro, *J. Am. Chem. Soc.*, 2010, **132**, 2140-2141.
20. D. E. Koutsonikolas, S. P. Kaldis, S. D. Sklari, G. Pantoleontos, V. T. Zaspalis and G. P. Sakellaropoulos, *Microporous Mesoporous Mater.*, 2010, **132**, 276-281.
21. K. Xu, C. Yuan, J. Caro and A. Huang, *J. Membr. Sci.*, 2016, **511**, 1-8.
22. L. Zhou, J. Yang, G. Li, J. Wang, Y. Zhang, J. Lu and D. Yin, *Int. J. Hydrogen Energy* 2014, **39**, 14949-14954.
23. A. Huang and J. Caro, *Chem. Commun.*, 2010, **46**, 7748-7750.